Accepted Manuscript

An immersed weak Galerkin method for elliptic interface problems

Lin Mu, Xu Zhang

PII: S0377-0427(18)30500-4

DOI: https://doi.org/10.1016/j.cam.2018.08.023

Reference: CAM 11860

To appear in: Journal of Computational and Applied

Mathematics

Received date: 20 February 2018 Revised date: 27 July 2018

https://doi.org/10.1016/j.cam.2018.08.023



This is a PDF file of an unedited manuscript that has been accepted for publication. As a service to our customers we are providing this early version of the manuscript. The manuscript will undergo copyediting, typesetting, and review of the resulting proof before it is published in its final form. Please note that during the production process errors may be discovered which could affect the

Please cite this article as: L. Mu, X. Zhang, An immersed weak Galerkin method for elliptic

interface problems, Journal of Computational and Applied Mathematics (2018),

content, and all legal disclaimers that apply to the journal pertain.



An Immersed Weak Galerkin Method For Elliptic Interface Problems

Lin Mu¹

Computer Science and Mathematics Division, Oak Ridge National Laboratory, Oak Ridge, TN 37831, USA (mul1@ornl.gov).

Xu Zhang²

Department of Mathematics and Statistics, Mississippi State University, Mississippi State, MS 39762, USA (xuzhang@math.msstate.edu)

Abstract

In this paper, we present an immersed weak Galerkin method for solving second-order elliptic interface problems. The proposed method does not require solution meshes to be aligned with the interface. Consequently, uniform Cartesian meshes can be used for nontrivial interfacial geometry. We show the existence and uniqueness of the numerical algorithm, and provide the error analysis in the energy norm. Numerical results are reported to demonstrate the performance of the method.

Keywords: immersed weak Galerkin, interface problems, Cartesian mesh, error estimate

1. Introduction

We consider the following elliptic interface equation

$$-\nabla \cdot (\beta \nabla u) = f, \text{ in } \Omega^- \cup \Omega^+, \tag{1.1}$$

$$u = g$$
, on $\partial \Omega$, (1.2)

where the domain $\Omega \subset \mathbb{R}^2$ is separated by an interface curve Γ into two subdomains Ω^+ and Ω^- . The diffusion coefficient $\beta(\mathbf{x})$ is discontinuous across the interface. Without loss of generality, we assume $\beta(\mathbf{x})$ is a piecewise constant function as follows

$$\beta(\mathbf{x}) = \begin{cases} \beta^-, & \text{if } \mathbf{x} \in \Omega^-, \\ \beta^+, & \text{if } \mathbf{x} \in \Omega^+. \end{cases}$$

The exact solution u is required to satisfy the following homogeneous jump conditions

$$\|u\|_{\Gamma} = 0. \tag{1.3}$$

$$[\beta \nabla u \cdot \mathbf{n}]|_{\Gamma} = 0, \tag{1.4}$$

where \mathbf{n} is the unit normal vector to the interface Γ . From now on, we define

$$v = \begin{cases} v^{-}(\mathbf{x}), & \text{if } \mathbf{x} \in \Omega^{-}, \\ v^{+}(\mathbf{x}), & \text{if } \mathbf{x} \in \Omega^{+}, \end{cases}$$

and denote the jump $\llbracket v \rrbracket |_{\Gamma} = v^+|_{\Gamma} - v^-|_{\Gamma}$.

¹This author's research was supported in part by the U.S. Department of Energy, Office of Advanced Scientific Computing Research, Applied Mathematics program under award number ERKJE45; and by the Laboratory Directed Research and Development program at the Oak Ridge National Laboratory, which is operated by UT-Battelle, LLC., for the U.S. Department of Energy under Contract DE-AC05-00OR22725.

²This author is supported in part by the National Science Foundation under Grant No. DMS-1720425.

Interface problems arise in many applications in science and engineering. The elliptic problem (1.1) - (1.4) represents a typical interface model problem since it captures many fundamental physical phenomena. To solve interface problems, in general, there are two classes of numerical methods. The first class of methods use interface-fitted meshes, i.e., the solution mesh is tailored to fit the interface. Methods of this type include classical finite element methods (FEM) [6, 10], discontinuous Galerkin methods [3, 41], and the virtual element methods [4, 5]. The second class of methods use unfitted meshes which are independent of the interface. Structured uniform meshes such as Cartesian meshes are often utilized in these methods. The advantages of unfitted-mesh methods often emerge when the interface is geometrically complicated for which a high-quality body-fitting mesh is difficult to generate; or the dynamic simulation involves a moving interface, which requires repeated mesh generation. In the past decades, many numerical methods based on unfitted meshes have been developed. For instance, the immersed interface methods [23, 25], cut finite element methods [7, 15], multi-scale finite element methods [11, 21], extended finite element methods [12, 36], to name only a few.

The immersed finite element method (IFEM) is a class of unfitted mesh methods for interface problems. The main idea of IFEM is to locally adjust the approximation function instead of solution mesh to resolve the solution around the interface. The IFEM was first developed for elliptic interface problems [2, 8, 24, 27, 28] and was recently applied to other interface model problems such as elasticity system [34, 31], Stokes flow [1], parabolic moving interface problems [18, 29], etc. Recently, this *immersed* idea has also been used in various numerical algorithms in addition to classical conforming FEM, such as nonconforming IFEM [14, 22, 32], immersed Petrov-Galerkin methods [19, 20], immersed discontinuous Galerkin methods [17, 33], and immersed finite volume methods [9, 16, 43].

The weak Galerkin (WG) methods are a new class of finite element discretizations for solving partial differential equations (PDE) [37, 42]. In the framework of the WG method, classical differential operators are replaced by generalized differential operators as distributions. Unlike the classical FEM that impose continuity in the approximation space, the WG methods enforce the continuity weakly in the formulation using generalized discrete weak derivatives and parameter-free stabilizers. The WG methods are naturally extended from the standard FEM for functions with discontinuities, and thus are more advantageous over FEM in several aspects [35, 39]. For instance, high-order WG spaces are usually constructed more conveniently than conforming FEM spaces since there is no continuity requirement on the approximation spaces. Also, the relaxation of the continuity requirement enables easy implementation of WG methods on polygonal meshes, and more flexibility for *h*- and *p*- adaptation. Moreover, the weak Galerkin methods is absolutely stable and there is no tuning parameter in the scheme, which is different from interior penalty discontinuous Galerkin (IPDG) methods.

Recently, the WG methods have been studied for elliptic interface problems [38, 40]. These WG methods are require interface-fitted meshes. In this article, we will develop an immersed weak Galerkin (IWG) methods for elliptic interface problems on unfitted meshes. The proposed IWG method combines the advantages from both immersed finite element approximation and the weak Galerkin formulation. One apparent advantage of our IWG method over standard WG method is that it can be applied on unfitted meshes such as Cartesian meshes for solving elliptic interface problems. Comparing with the immersed IPDG methods [17, 33], the matrix assembling in the IWG method assembles is more efficiently because all computation can be done locally within an element without exchange information from neighboring elements.

The rest of the article is organized as follows. In Section 2, we recall the P_1 immersed finite element spaces that will be used to construct the WG approximation spaces. In Section 3, we introduce the IWG algorithm and discuss the well-posedness of the discretized problem. Section 4 is dedicated to the error analysis of the IWG algorithm. We will show that the errors measured in energy norm obey the optimal rate of convergence with respect to the polynomial degree of approximation space. In Section 5, we provide several numerical examples to demonstrate features of our IWG method.

2. Immersed Finite Element Functions and Weak Galerkin Methods

In this section, we introduce notations to be used in this article. We will also review the basic ideas of weak Galerkin methods and immersed finite element spaces. Throughout this paper, we adopt notations of standard Sobolev spaces. For m > 1, and any subset $G \subset \Omega$ that is cut through by the interface Γ , we define the following Hilbert spaces

$$\tilde{H}^m(G) = \{ u \in H^1(G) : u|_{G \cap \Omega^s} \in H^m(G \cap \Omega^s), \ s = + \text{ or } - \}$$

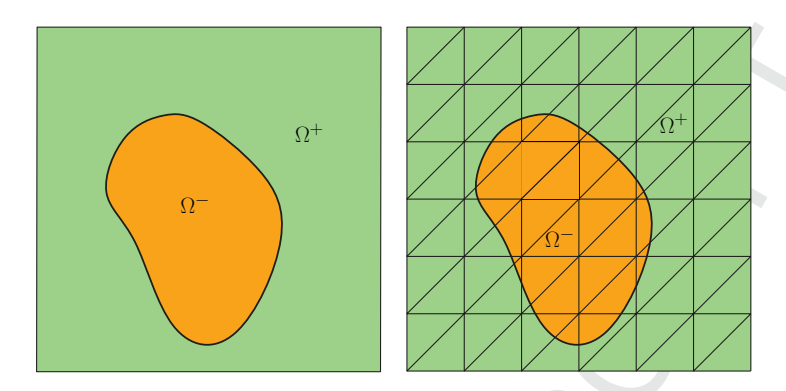


Figure 1: Plots of interface Γ and a Cartesian triangular mesh.

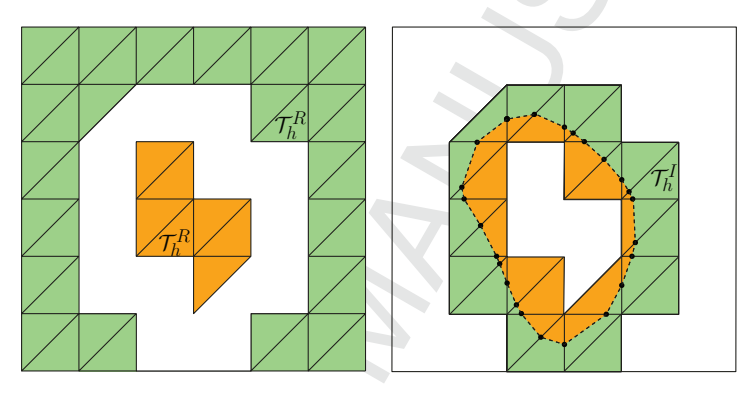


Figure 2: Plots of regular elements \mathcal{T}_h^R and interface elements \mathcal{T}_h^I .

equipped the following norm and semi-norm:

$$||u||_{\tilde{H}^m(G)} = ||u||_{m,G\cap\Omega^+} + ||u||_{m,G\cap\Omega^-}, \quad |u|_{\tilde{H}^m(G)} = |u|_{m,G\cap\Omega^+} + |u|_{m,G\cap\Omega^-}.$$

2.1. Immersed Finite Element Spaces

Let \mathcal{T}_h be a shape-regular triangular mesh of the domain Ω . For every element $T \in \mathcal{T}_h$, we denote by h_T its diameter. The mesh size of \mathcal{T}_h is defined by $h = \max_{T \in \mathcal{T}_h} h_T$. Since the mesh \mathcal{T}_h is independent of the interface, we often use Cartesian triangular mesh for simplicity, see Figure 1. The interface Γ may intersect with some elements in \mathcal{T}_h , which are called interface elements. The rest of elements are called regular elements, see Figure 2. The collections of interface elements and regular elements, are denoted by \mathcal{T}_h^I and \mathcal{T}_h^R , respectively. Denote by \mathcal{E}_h the set of all edges in \mathcal{T}_h , and let $\mathcal{E}_h^0 = \mathcal{E}_h \setminus \partial \Omega$ be the set of all interior edges.

Without of generality, we assume that \mathcal{T}_h satisfies the following hypotheses, when the mesh size h is small enough:

- (H1). The interface Γ cannot intersect the boundary of an element at more than two points unless a boundary edge of the element is part of Γ .
- (H2). If Γ intersects the boundary of an element at two points, these points must be on different edges of this element.
- (H3). The interface Γ is a piecewise C^2 -function, and the mesh \mathcal{T}_h is formed such that the subset of Γ in every interface element $T \in \mathcal{T}_h^I$ is C^2 -continuous.
- (H4). When the mesh size h is small enough, the number of interface elements is of order $O(h^{-1})$.

To be self-contained, we briefly recall the linear IFE space introduced in [26, 27]. Let $T \in \mathcal{T}_h^I$ be an interface element. Denote the three vertices of T by A_1 , A_2 , and A_3 . The interface curve Γ cut the boundary of T at two points D, E. The line segment \overline{DE} divides the element T into two sub-elements T^- and T^+ . See Figure 3 for a typical interface triangle.

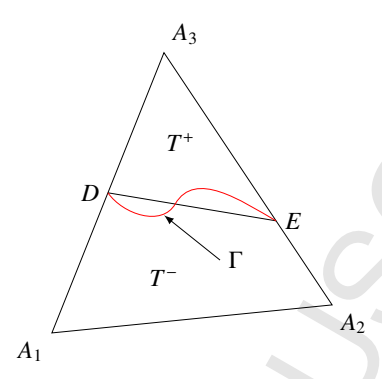


Figure 3: A typical triangular interface element.

The linear IFE functions are constructed by incorporating the interface jump conditions. Specifically, three linear IFE shape functions ϕ_i , i = 1, 2, 3 associated with the vertices of A_i , i = 1, 2, 3 are constructed in the form of

$$\phi_{i}(x,y) = \begin{cases} \phi_{i}^{+}(x,y) = a_{i}^{+} + b_{i}^{+}x + c_{i}^{+}y, & \text{if } (x,y) \in T^{+}, \\ \phi_{i}^{-}(x,y) = a_{i}^{-} + b_{i}^{-}x + c_{i}^{-}y, & \text{if } (x,y) \in T^{-}, \end{cases}$$
(2.1)

satisfying the following conditions:

• nodal value condition

$$\phi_i(A_i) = \delta_{ij}, \quad i, j = 1, 2, 3.$$
 (2.2)

• continuity of the function

$$[\![\phi_i(D)]\!] = 0, \quad [\![\phi_i(E)]\!] = 0.$$
 (2.3)

• continuity of normal component of flux

$$\left[\left[\beta \frac{\partial \phi_i}{\partial n}\right]\right]_{\overline{DE}} = 0. \tag{2.4}$$

It has been shown in [26] that conditions specified in (2.2) - (2.4) can uniquely determine these shape functions in (2.1). Then, on each interface element $T \in \mathcal{T}_h^I$, we define the local IFE space

$$\tilde{P}_1(T) = span\{\phi_1, \phi_2, \phi_3\}.$$
 (2.5)

2.2. Weak Functions

The weak Galerkin method takes finite element functions in the form of two components, one in the interior and the other on the boundary. This means for a weak function ν defined on an element T,

$$v = \begin{cases} v_0, & \text{in } T, \\ v_b, & \text{on } \partial T. \end{cases}$$

For simplicity, we shall write v as $v = \{v_0, v_b\}$ in short.

We consider the following weak Galerkin finite element space

$$V_h := \left\{ v = \{ v_0, v_b \} : \ v_0|_T \in P_1(T), \text{ if } T \in \mathcal{T}_h^R, v_0|_T \in \tilde{P}_1(T), \text{ if } T \in \mathcal{T}_h^I; \ v_b|_e \in P_0(e), e \subset \mathcal{E}_h \right\}.$$

Here $P_1(T)$ is the standard linear polynomial space, and $\tilde{P}_1(T)$ is the linear immersed finite element space on T defined in (2.5). The $P_0(e)$ is the standard piecewise constant function on the edge e. Let V_h^0 be the subspace of V_h consisting of finite element functions with vanishing boundary value:

$$V_h^0 = \{ v \in V_h : v_b = 0 \text{ on } \partial \Omega \}.$$

On each element $T \in \mathcal{T}_h$, define the projection operator Q_h by

$$Q_hu=\{Q_0u,Q_bu\}\in V_h.$$

Here, Q_0 is the Lagrange interpolation or the L^2 project from C(T) to $P_1(T)$ if T is a regular element, and Q_0 is the Lagrange interpolation from C(T) to $\tilde{P}_1(T)$ if T is an interface element. Q_b is the L^2 projection from $L^2(e)$ to $P_0(e)$ for every edge e.

The immersed weak Galerkin method for the problem (1.1)-(1.4) is to seek: $u_h = \{u_{h0}, u_{hb}\} \in V_h$ such that

$$A(u_h, v) = (f, v_0), \ \forall v \in V_h^0,$$
 (2.6)

where the bilinear form A(u, v) is defined as

$$A(u, v) = \sum_{T \in \mathcal{T}_h} \left((\beta \nabla u_0, \nabla v_0)_T - \langle Q_b (\beta \nabla u_0 \cdot \mathbf{n}), v_0 - v_b \rangle_{\partial T} - \langle Q_b (\beta \nabla v_0 \cdot \mathbf{n}), u_0 - u_b \rangle_{\partial T} + \rho h^{-1} \langle Q_b u_0 - u_b, Q_b v_0 - v_b \rangle_{\partial T} \right),$$

$$(2.7)$$

where ρ is a positive constant.

Remark 2.1. On every regular element $T \in \mathcal{T}_h^R$ and $e \subset \partial T$, we have $Q_b(\beta \nabla \phi_0 \cdot \mathbf{n}) = \beta \nabla \phi_0 \cdot \mathbf{n}$ simply because $\beta \nabla \phi_0 \cdot \mathbf{n}$ is a constant.

3. Well-posedness of Numerical Algorithm

In this section, we present the existence and uniqueness of the proposed immersed weak Galerkin method. First, we define the energy norm by

$$\|\|v\|\|^2 = \sum_{T \in \mathcal{T}_h^R \cup \mathcal{T}_h^I} (\|\beta^{1/2} \nabla v_0\|_T^2 + \rho h^{-1} \|Q_b v_0 - v_b\|_{\partial T}^2).$$

Lemma 3.1. The following inequality holds on every element $T \in \mathcal{T}_h$

$$\|v_0 - v_b\|_{\partial T}^2 \le h\|\nabla v_0\|_T^2 + \|Q_b v_0 - v_b\|_{\partial T}^2, \quad \forall v \in V_h.$$
(3.1)

Proof. We note that the inequality (3.1) is a standard estimate for $T \in \mathcal{T}_h^R$. On an interface element $T \in \mathcal{T}_h^I$, we note that $v_0 \in H^1(T)$. Therefore, applying the triangular inequality and trace inequality yields

$$\|v_0 - v_b\|_{\partial T}^2 \le \|v_0 - Q_b v_0\|_{\partial T}^2 + \|Q_b v_0 - v_b\|_{\partial T}^2 \le h \|\nabla v_0\|_T^2 + \|Q_b v_0 - v_b\|_{\partial T}^2.$$

Lemma 3.2. For all $v \in V_h$, $T \in \mathcal{T}_h$, and $e \subset \partial T$, the following inequality holds,

$$||Q_b v||_e \le ||v||_e \quad \forall v \in V_h.$$
 (3.2)

Proof. By the definition of Q_b and Cauchy-Schwartz inequality, we obtain

$$||Q_b v||_e^2 = \langle Q_b v, Q_b v \rangle_e = \langle v, Q_b v \rangle_e \le ||v||_e ||Q_b v||_e.$$

Theorem 3.1. The immersed weak Galerkin method (2.6) has a unique solution provided that ρ is big enough.

Proof. We show this well-posedness result by proving the continuity and coercivity of the bilinear form. For the continuity, we have

$$\begin{split} A(w,v) &= \sum_{T \in \mathcal{T}_{h}^{R} \cup \mathcal{T}_{h}^{I}} \left((\beta \nabla w_{0}, \nabla v_{0})_{T} - \langle Q_{b}(\beta \nabla w_{0} \cdot \mathbf{n}), v_{0} - v_{b} \rangle_{\partial T} \right. \\ &- \langle Q_{b}(\beta \nabla v_{0} \cdot \mathbf{n}), w_{0} - w_{b} \rangle_{\partial T} + h^{-1} \rho \langle Q_{b} w_{0} - w_{b}, Q_{b} v_{0} - v_{b} \rangle_{\partial T} \right) \\ &= \sum_{T \in \mathcal{T}_{h}^{R} \cup \mathcal{T}_{h}^{I}} \left((\beta \nabla w_{0}, \nabla v_{0})_{T} - \langle Q_{b}(\beta \nabla w_{0} \cdot \mathbf{n}), Q_{b} v_{0} - v_{b} \rangle_{\partial T} \right. \\ &- \langle Q_{b}(\beta \nabla v_{0} \cdot \mathbf{n}), Q_{b} w_{0} - w_{b} \rangle_{\partial T} + h^{-1} \rho \langle Q_{b} w_{0} - w_{b}, Q_{b} v_{0} - v_{b} \rangle_{\partial T} \right) \\ &\leq \sum_{T} \left(||\beta^{1/2} \nabla w_{0}||_{T} ||\beta^{1/2} \nabla v_{0}||_{T} + (h||\beta^{1/2} \nabla w_{0} \cdot \mathbf{n}||_{\partial T}^{2})^{1/2} (\beta h^{-1} ||Q_{b} v_{0} - v_{b}||_{e}^{2})^{1/2} \\ &+ (h||\beta^{1/2} \nabla v_{0} \cdot \mathbf{n}||_{\partial T}^{2})^{1/2} (\beta h^{-1} ||Q_{b} w_{0} - w_{b}||_{e}^{2})^{1/2} + (h^{-1} \rho ||Q_{b} v_{0} - v_{b}||_{\partial T}^{2})^{1/2} (h^{-1} \rho ||Q_{b} w_{0} - w_{b}||_{\partial T}^{2})^{1/2} \right) \\ &\leq \sum_{T} \left(||\beta^{1/2} \nabla w_{0}||_{T} ||\beta^{1/2} \nabla v_{0}||_{T} + ||\beta^{1/2} \nabla w_{0}||_{T} (\beta h^{-1} ||Q_{b} v_{0} - v_{b}||_{e}^{2})^{1/2} \\ &+ ||\beta^{1/2} \nabla v_{0}||_{T} (\beta h^{-1} ||Q_{b} w_{0} - w_{b}||_{e}^{2})^{1/2} + (h^{-1} \rho ||Q_{b} v_{0} - v_{b}||_{\partial T}^{2})^{1/2} (h^{-1} \rho ||Q_{b} w_{0} - w_{b}||_{\partial T}^{2})^{1/2} \right) \\ &\leq C ||w|| ||v||. \end{split}$$

Then, we show the coercivity of the bilinear form. Note that

$$A(v,v) = \sum_{T \in \mathcal{T}_{-}} \left(\|\beta^{1/2} \nabla v_0\|_T^2 - 2\langle Q_b(\beta \nabla v_0 \cdot \mathbf{n}), v_0 - v_b \rangle_{\partial T} + \rho h^{-1} \|Q_b v_0 - v_b\|_{\partial T}^2 \right). \tag{3.3}$$

We have for $T \in \mathcal{T}_h^R \cup \mathcal{T}_h^I$

$$\begin{split} 2 \left\langle Q_{b}(\beta \nabla v_{0} \cdot \mathbf{n}), v_{0} - v_{b} \right\rangle_{\partial T} &= 2 \left\langle Q_{b}(\beta \nabla v_{0} \cdot \mathbf{n}), Q_{b}v_{0} - v_{b} \right\rangle_{\partial T} \\ &\leq 2 \left(h \|Q_{b}(\beta^{1/2} \nabla v_{0} \cdot \mathbf{n})\|_{\partial T}^{2} \right)^{1/2} \left(\beta h^{-1} \|Q_{b}v_{0} - v_{b}\|_{\partial T}^{2} \right)^{1/2} \\ &\leq 2 \left(\frac{h \|\beta^{1/2} \nabla v_{0} \cdot \mathbf{n}\|_{\partial T}^{2}}{2\epsilon} \right) + 2 \left(\frac{\beta \epsilon h^{-1} \|Q_{b}v_{0} - v_{b}\|_{\partial T}^{2}}{2} \right) \\ &= \frac{h \|\beta^{1/2} \nabla v_{0} \cdot \mathbf{n}\|_{\partial T}^{2}}{\epsilon} + \epsilon \beta h^{-1} \|Q_{b}v_{0} - v_{b}\|_{\partial T}^{2} \\ &\leq (1/\epsilon) \|\beta^{1/2} \nabla v_{0}\|_{T}^{2} + \epsilon \beta h^{-1} \|Q_{b}v_{0} - v_{b}\|_{\partial T}^{2}. \end{split}$$

Substituting the above inequality into (3.3), we obtain

$$A(v,v) \ge \sum_{T \in \mathcal{T}_b} (1 - 1/\epsilon) \|\beta^{1/2} \nabla v_0\|_T^2 + (\rho - \epsilon \beta_{\max}) h^{-1} \|Q_b v_0 - v_b\|_{\partial T}^2.$$

Choosing $\epsilon = 2$ and $\rho > 2\beta_{\text{max}}$ completes the proof of the coercivity.

4. Error Analysis

In this section, we derive the a priori error estimate for the IWG method (2.6) in the energy norm. First, we recall some trace inequalities on regular elements and interface elements. Let $T \in \mathcal{T}_h^R$ be a regular element and e be an edge of T. The standard trace inequality holds for every function $v \in H^1(T)$:

$$||v||_e^2 \le C \left(h_T^{-1} ||v||_{0,T}^2 + h_T ||\nabla v||_{0,T}^2 \right). \tag{4.1}$$

If $T \in \mathcal{T}_h^I$ is an interface element, the following lemma provides the trace inequalities of IFE functions [30].

Lemma 4.1. There exists a constant C independent of the interface location such that for every linear IFE function $v \in \tilde{P}_1(T)$ the following inequalities hold:

$$\|\partial_{p}v\|_{0,e} \leq Ch^{1/2}|T|^{-1/2}\|\sqrt{\beta}\nabla v\|_{0,T}, \ p = x, y$$

$$\|\beta\nabla v \cdot \mathbf{n}_{e}\|_{0,e} \leq Ch^{1/2}|T|^{-1/2}\|\sqrt{\beta}\nabla v\|_{0,T}.$$
(4.2)

$$\|\beta \nabla v \cdot \mathbf{n}_e\|_{0,e} \le C h^{1/2} |T|^{-1/2} \|\sqrt{\beta} \nabla v\|_{0,T}.$$
 (4.3)

The next two lemmas provide the interpolation error estimates for linear IFE spaces [26, 30].

Lemma 4.2. Let $T \in \mathcal{T}_h^I$ be an interface element. There exists a constant C, independent of interface location, such that the interpolation $I_h u$ in the IFE space $\tilde{P}_1(T)$ has the following error bound:

$$||u - I_h u||_{0,T} + h||u - I_h u||_{1,T} \le Ch^2 ||u||_{\tilde{H}^2(T)}, \quad \forall u \in \tilde{H}^2(T). \tag{4.4}$$

Lemma 4.3. For every $u \in \tilde{H}^3(\Omega)$ satisfying the interface jump conditions, there exists a constant C independent of the interface such that its interpolation I_hu in the IFE space V_h has the following bound:

$$\|\beta \nabla (u - I_h u)|_T \cdot \mathbf{n}_e\|_e^2 \le C \Big(h^2 \|u\|_{\tilde{H}^3(\Omega)}^2 + h \|u\|_{\tilde{H}^2(T)}^2 \Big), \tag{4.5}$$

where T is an interface element and e is one of its interface edge.

Next, we present some lemmas that will be used in our error analysis.

Lemma 4.4. There exists a constant C such that

$$|S(Q_h w, v)| \le Ch||w||_{\tilde{H}^2(\Omega)} ||v||, \quad \forall w \in \tilde{H}^2(\Omega), \quad \forall v \in V_h$$

$$\tag{4.6}$$

where $S(Q_h w, v) = \sum_T h^{-1} \langle Q_b Q_0 w - Q_b w, Q_b v_0 - v_b \rangle_{\partial T}$.

Proof. Using the Cauchy-Schwarz inequality, trace inequality, and the interpolation error bound (4.4), we have

$$\begin{split} |S(Q_h w, v)| &= \left| \sum_{T \in \mathcal{T}_h^R \cup \mathcal{T}_h^I} h^{-1} \langle Q_b(Q_0 w) - Q_b w, Q_b v_0 - v_b \rangle_{\partial T} \right| = \left| \sum_{T \in \mathcal{T}_h^R} h^{-1} \langle Q_0 w - w, Q_b v_0 - v_b \rangle_{\partial T} \right| \\ &\leq C \bigg(\sum_{T \in \mathcal{T}_h^R} h^{-2} ||Q_0 w - w||_T^2 + ||\nabla (Q_0 w - w)||_T^2 \bigg)^{1/2} \bigg(\sum_{T \in \mathcal{T}_h^R} h^{-1} ||Q_b v_0 - v_b||_{\partial T}^2 \bigg)^{1/2} \\ &\leq C h ||w||_{\dot{H}^2(\Omega)} ||v||. \end{split}$$

Lemma 4.5. There exists a constant C such that

$$\sum_{T \in \mathcal{T}_h} \|Q_0 u - u\|_{\partial T}^2 \le C h^3 \|u\|_{\tilde{H}^2(\Omega)}^2. \tag{4.7}$$

Proof. Applying the trace inequality and the interpolation error bound (4.4), we have

$$||Q_0u - u||_{\partial T} \le C \left(h^{1/2}|Q_0u - u|_{1,T} + h^{-1/2}||Q_0u - u||_{0,T}\right) \le Ch^{3/2}||u||_{\tilde{H}^2(T)}.$$

Squaring both sides and summing over all elements lead to the estimate (4.7).

Lemma 4.6. Let $u_h = \{u_0, u_b\}$ and u be the solutions to problem (2.6) and (1.1)-(1.2), respectively. Let $Q_h u = \{Q_0 u, Q_b u\}$ be the projection of u to the finite element space V_h . Then, for every function $v \in V_h^0$, one has the following error equation

$$A(Q_h u - u_h, v) = L_u(v) + S(Q_h u, v), \tag{4.8}$$

where

$$L_{u}(v) = \sum_{T \in \mathcal{T}_{h}} \left(\langle u - Q_{0}u, \beta \nabla v_{0} \cdot \mathbf{n} - Q_{b}(\beta \nabla v_{0} \cdot \mathbf{n}) \rangle_{\partial T} + \langle \beta \nabla u \cdot \mathbf{n} - Q_{b}(\beta \nabla Q_{0}u \cdot \mathbf{n}), v_{0} - v_{b} \rangle_{\partial T} \right). \tag{4.9}$$

Proof. For any $v = (v_0, v_b) \in V_b^0$, we multiply (1.1) by v_0 to obtain

$$\begin{split} (f, v_0) &= \sum_{T \in T_h} (-\nabla \cdot \beta \nabla u, v_0)_T = \sum_{T \in T_h} \left(-\langle \beta \nabla u \cdot \mathbf{n}, v_0 \rangle_{\partial T} + (\beta \nabla u, \nabla v_0)_T \right) \\ &= \sum_{T \in T_h} \left(-\langle \beta \nabla u \cdot \mathbf{n}, v_0 \rangle_{\partial T} + \langle u, \beta \nabla v_0 \cdot \mathbf{n} \rangle_{\partial T} - (u, \nabla \cdot \beta \nabla v_0)_T \right) \\ &= \sum_{T \in T_h} \left(-\langle \beta \nabla u \cdot \mathbf{n}, v_0 \rangle_{\partial T} + \langle u, \beta \nabla v_0 \cdot \mathbf{n} \rangle_{\partial T} - (Q_0 u, \nabla \cdot \beta \nabla v_0)_T \right) \\ &= \sum_{T \in T_h} \left(-\langle \beta \nabla u \cdot \mathbf{n}, v_0 \rangle_{\partial T} + \langle u, \beta \nabla v_0 \cdot \mathbf{n} \rangle_{\partial T} - \langle Q_0 u, \beta \nabla v_0 \cdot \mathbf{n} \rangle_{\partial T} + (\nabla Q_0 u, \beta \nabla v_0)_T \right) \\ &= \sum_{T \in T_h} \left((\beta \nabla Q_0 u, \nabla v_0)_T - \langle Q_0 u, \beta \nabla v_0 \cdot \mathbf{n} \rangle_{\partial T} + \langle u, \beta \nabla v_0 \cdot \mathbf{n} \rangle_{\partial T} - \langle \beta \nabla u \cdot \mathbf{n}, v_0 - v_b \rangle_{\partial T} \right). \end{split}$$

The last equation is because v_b is a constant on every edge, and the flux $\beta \nabla u \cdot \mathbf{n}$ is continuous. Then by the definition of the bilinear form (2.7), we have

$$A(Q_{h}u, v) = (f, v_{0}) + \sum_{T \in \mathcal{T}_{h}} \left(\langle u - Q_{0}u, Q_{b}(\beta \nabla v_{0} \cdot \mathbf{n}) - \beta \nabla v_{0} \cdot \mathbf{n} \rangle_{\partial T} + \langle \beta \nabla u \cdot \mathbf{n} - Q_{b}(\beta \nabla Q_{0}u \cdot \mathbf{n}), v_{0} - v_{b} \rangle_{\partial T} + \rho h^{-1} \langle Q_{b}Q_{0}u - Q_{b}u, Q_{b}v_{0} - v_{b} \rangle_{\partial T} \right).$$

$$(4.10)$$

Subtracting (2.6) from the above equation, it is obtained that

$$A(Q_{h}u - u_{h}, v) = \sum_{T \in \mathcal{T}_{h}} \left(\langle u - Q_{0}u, Q_{b}(\beta \nabla v_{0} \cdot \mathbf{n}) - \beta \nabla v_{0} \cdot \mathbf{n} \rangle_{\partial T} + \langle \beta \nabla u \cdot \mathbf{n} - Q_{b}(\beta \nabla Q_{0}u \cdot \mathbf{n}), v_{0} - v_{b} \rangle_{\partial T} \right)$$

$$+ \rho h^{-1} \langle Q_{b}Q_{0}u - Q_{b}u, Q_{b}v_{0} - v_{b} \rangle_{\partial T}$$

$$= L_{u}(v) + S(Q_{h}u, v),$$

which completes the proof.

Lemma 4.7. The linear form $L_u(v)$ in (4.9) has the following error estimate

$$L_u(v) \le Ch||u||_{\tilde{H}^3(\Omega)} |||v|||,$$
 (4.11)

where the constant C is independent of the interface location.

Proof. In (4.9), we denote $L_u(v) = I + II$. By Cauchy-Schwartz inequality, (3.2), and (4.7), we obtain

$$\begin{split} I &= \sum_{T} \langle u - Q_0 u, Q_b (\beta \nabla v_0 \cdot \mathbf{n}) - \beta \nabla v_0 \cdot \mathbf{n} \rangle_{\partial T} \\ &\leq \sum_{T} (h^{1/2} || Q_b (\beta \nabla v_0 \cdot \mathbf{n}) ||_{\partial T} + h^{1/2} || \beta \nabla v_0 \cdot \mathbf{n} ||_{\partial T}) (h^{-1/2} || Q_0 u - u ||_{\partial T}) \\ &\leq C h || u ||_{\dot{H}^2(\Omega)} \sum_{T} || \beta^{1/2} \nabla v_0 ||_{T} \\ &\leq C h || u ||_{\dot{B}^2(\Omega)} || v |||_{\bullet}. \end{split}$$

Next, by the trace inequality

$$II = \sum_{T} \langle \beta \nabla u \cdot \mathbf{n} - Q_{b}(\beta \nabla Q_{0}u \cdot \mathbf{n}), v_{0} - v_{b} \rangle_{\partial T}$$

$$= \sum_{T} \langle \beta \nabla u \cdot \mathbf{n} - Q_{b}(\beta \nabla Q_{0}u \cdot \mathbf{n}), v_{0} - Q_{b}v_{0} \rangle_{\partial T} + \langle \beta \nabla u \cdot \mathbf{n} - Q_{b}(\beta \nabla Q_{0}u \cdot \mathbf{n}), Q_{b}v_{0} - v_{b} \rangle_{\partial T}$$

$$= \sum_{T} \langle \beta \nabla u \cdot \mathbf{n} - Q_{b}(\beta \nabla u \cdot \mathbf{n}), v_{0} - Q_{b}v_{0} \rangle_{\partial T} + \langle \beta \nabla u \cdot \mathbf{n} - \beta \nabla Q_{0}u \cdot \mathbf{n}, Q_{b}v_{0} - v_{b} \rangle_{\partial T}$$

$$\leq \sum_{T} (h^{1/2} ||\beta \nabla u \cdot \mathbf{n} - Q_{b}(\beta \nabla u \cdot \mathbf{n})||_{\partial T})(h^{-1/2} ||v_{0} - Q_{b}v_{0}||_{\partial T})$$

$$+ (h^{1/2} ||\beta \nabla u \cdot \mathbf{n} - \beta \nabla Q_{0}u \cdot \mathbf{n}||_{\partial T})(h^{-1/2} ||Q_{b}v_{0} - v_{b}||_{\partial T})$$

$$\leq Ch||u||_{\dot{H}^{2}(\Omega)} \sum_{T} ||\nabla v_{0}||_{T} + \left(\sum_{T \in \mathcal{T}_{h}^{I}} (h^{3} ||u||_{\dot{H}^{3}(\Omega)}^{2} + h^{2} ||u||_{\dot{H}^{2}(T)}^{2}) + \sum_{T \in \mathcal{T}_{h}^{R}} h^{2} ||u||_{\dot{H}^{2}(T)}^{2}\right)^{1/2} |||v|||$$

$$< h||u||_{\dot{H}^{3}(\Omega)} ||v|||.$$

In the last step, we use the hypotheses (H4) that the number of interface elements is of order $O(h^{-1})$. Combining the error bounds for I and II, we obtain (4.11).

Now we are ready to prove our main result.

Theorem 4.1. Let $Q_h u$ and u_h be solutions to (4.9) and (2.6), respectively. Then the following error estimate holds

$$||Q_h u - u_h|| \le Ch||u||_{\tilde{H}^3(\Omega)},$$
 (4.12)

where the constant is independent of the interface location.

Proof. Taking $v = Q_h u - u_h$ in error equation (4.8), and then from the above estimates, (4.6), and combining with the coercivity of $A(\cdot, \cdot)$, we have

$$\begin{split} c\|\|Q_h u - u_h\|\|^2 & \leq & A(Q_h u - u_h, Q_h u - u_h) \\ & = & L_u(Q_h u - u_h) + S(Q_h u, Q_h u - u_h) \\ & \leq & Ch\|u\|_{\tilde{H}^3(\Omega)} \|\|Q_h u - u_h\|\| + Ch\|u\|_{\tilde{H}^2(\Omega)} \|\|Q_h u - u_h\|\| \\ & \leq & Ch\|u\|_{\tilde{H}^3(\Omega)} \|\|Q_h u - u_h\|\|. \end{split}$$

Remark 4.1. In the error estimates (4.11) and (4.12), we need to assume that the regularity of the solution is piecewise H^3 , which is usually higher than the usual piecewise H^2 assumption for numerical methods based on linear polynomials. However, this is only necessary for theoretical error analysis. In computation, piecewise H^2 assumption is sufficient to gain optimal convergence rate.

9

N	DOF	$ e_0 _{L^{\infty}}$	Order	$ e_b _{L^{\infty}}$	Order	$ e_0 _{L^2}$	Order	$ e_0 _{H^1}$	Order
16	2.34E+3	1.74E-2		1.13E-2		2.99E-3		1.04E-1	
32	9.28E+3	5.21E-3	1.74	6.57E-2	0.78	7.81E-4	1.93	4.89E-2	1.08
64	3.70E+4	1.54E-3	1.75	4.06E-3	0.69	1.99E-4	1.97	2.44E-2	1.00
128	1.48E+5	4.34E-5	1.83	1.90E-3	1.09	5.11E-5	1.96	1.25E-2	0.97
256	5.90E+5	1.13E-4	1.94	9.90E-4	0.94	1.28E-5	2.00	6.28E-3	0.99
512	2.26E+6	3.16E-5	1.84	5.05E-3	0.97	3.22E-6	1.99	3.15E-3	1.00
1024	9.44E+6	7.89E-6	2.00	2.63E-4	0.94	8.09E-7	1.99	1.57E-3	1.01

Table 1: Errors of Immersed WG methods Circle Interface for $\beta^- = 1$, $\beta^+ = 1000$

5. Numerical Examples

In this section, we report some numerical examples to validate our theoretical results. Furthermore, we will report the convergence test of the numerical solution in other norms. We write the exact solution in $u = (u_0, u_b)$, and write the IWG solution in $u_h = (u_{0h}, u_{bh})$. For simplicity, we also define the errors

$$e_0 = u_0 - u_{0h}, \quad e_b = u_b - u_{bh}.$$

We will test the L^{∞} , L^2 , and semi- H^1 norms of e_0 , and L^{∞} norm of e_b in the following examples.

$$||e_0||_{L^2} = \left(\sum_{T \in \mathcal{T}_h} ||u - u_0||_T^2\right)^{1/2}, \quad |e_0|_{H^1} = \left(\sum_{T \in \mathcal{T}_h} ||\nabla (u - u_0)||_T^2\right)^{1/2},\tag{5.1}$$

$$||e_0||_{L^{\infty}} = \max_{x \in \mathcal{N}_h} ||u_0(x) - u_{0h}(x)||, \quad ||e_b||_{L^{\infty}} = \max_{x \in \mathcal{M}_h} ||u_b(x) - u_{bh}(x)||,$$
(5.2)

where \mathcal{N}_h and \mathcal{M}_h denote the set of nodes of the mesh, and the set of midpoints of all edges of the mesh, respectively. We note that the semi- H^1 norm of e_0 is equivalent to the energy norm that we considered in the analysis. Thus, one can expect the errors measured by them give the same convergence rates. In all the numerical experiments, we take $\rho = 10\beta_{max}$.

5.1. Example 1

We first consider a bench mark example for the elliptic interface problem which has been tested in many articles [30, 33]. Let $\Omega = (-1, 1) \times (-1, 1)$, which is divided into two subdomains Ω^- and Ω^+ by a circular interface Γ centered at origin with radius $r_0 = \pi/5$ such that $\Omega^- = \{(x, y) : x^2 + y^2 < r_0^2\}$ and $\Omega^+ = \{(x, y) : x^2 + y^2 > r_0^2\}$. Functions f and g are computed such that the analytical solution is described as follows:

$$u(x,y) = \begin{cases} \frac{1}{\beta^{-}} r^{\alpha}, & (x,y) \in \Omega^{-} \\ \frac{1}{\beta^{+}} r^{\alpha} + \left(\frac{1}{\beta^{-}} - \frac{1}{\beta^{+}}\right) r_{0}^{\alpha} & (x,y) \in \Omega^{+}, \end{cases}$$

$$(5.3)$$

where $r = \sqrt{x^2 + y^2}$ and $\alpha = 5$. We use the uniform Cartesian triangular meshes which is obtained by first partitioning the domain into $N \times N$ congruent rectangles and then connecting the top-left and bottom-right diagonal in every rectangle. We only report numerical performance for large coefficient contrasts $(\beta^-, \beta^+) = (1,1000)$ and $(\beta^-, \beta^+) = (1000,1)$. We also have tested some small coefficient jumps, and the numerical results are similar, hence we omit them in the paper. The numerical errors and convergence rates for these two cases are reported in Table 1 and Table 2, respectively. The numerical solutions on the 128×128 mesh are plotted in Figure 4. From these tables, we can observe clearly that the error e_0 in semi- H^1 norm converges optimally which confirms our theoretical analysis. Moreover, e_0 in L^2 and L^∞ norms also converge in second-order, which is considered as optimal. The boundary error e_b in L^∞ norm seems to converge in first order, which is anticipated as we use the piecewise constant approximation for u_b .

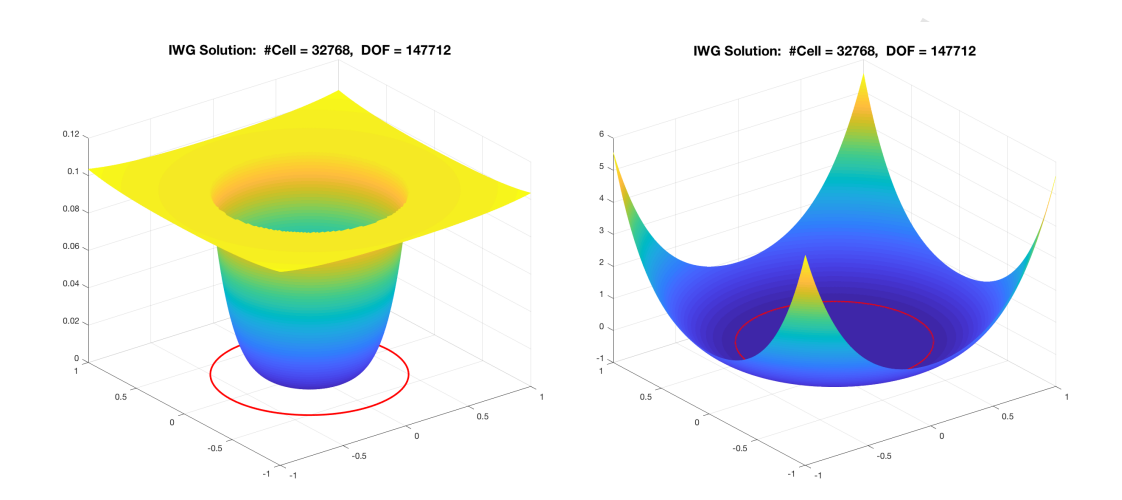


Figure 4: Immersed Weak Galerkin solutions for Example 1 with $(\beta^-, \beta^+) = (1, 1000)$, and $(\beta^-, \beta^+) = (1000, 1)$

N	DOF	$ e_0 _{L^\infty}$	Order	$ e_b _{L^{\infty}}$	Order	$ e_0 _{L^2}$	Order	$ e_0 _{H^1}$	Order
16	2.34E+3	1.81E-1		2.24E-2		3.13E-2		1.15E-0	
32	9.28E+3	4.83E-2	1.91	8.81E-3	1.35	7.89E-3	1.99	5.76E-1	1.00
64	3.70E+4	1.25E-3	1.95	4.62E-3	0.93	1.98E-3	2.00	2.88E-1	1.00
128	1.48E+5	3.17E-3	1.98	2.03E-3	1.19	4.94E-4	2.00	1.44E-1	1.00
256	5.90E+5	8.01E-4	1.99	1.02E-3	0.99	1.23E-4	2.00	7.20E-2	1.00
512	2.26E+6	2.01E-4	1.99	5.13E-4	1.00	3.09E-5	2.00	3.60E-2	1.00
1024	9.44E+6	5.04E-5	2.00	2.65E-4	0.96	7.73E-6	2.00	1.80E-2	1.00

Table 2: Errors of Immersed WG methods Circle Interface for $\beta^- = 1000$, $\beta^+ = 1$

5.2. Example 2

In this example, we test our numerical algorithm for a more complicated interface curve. We let $\Omega = (-1, 1) \times (-1, 1)$, and the interface is determined by the following level-set function:

$$\Gamma(x,y) = (x^2 + y^2)^2 (1 + 0.4\sin(6\arctan(\frac{y}{x}))) - 0.3.$$
 (5.4)

The subdomains are defined as $\Omega^+ = \{(x, y) : \Gamma(x, y) > 0\}$, and $\Omega^- = \{(x, y) : \Gamma(x, y) < 0\}$. The exact solution is chosen as:

$$u = \begin{cases} \frac{1}{\beta^{-}} \Gamma(x, y), & (x, y) \in \Omega^{-} \\ \frac{1}{\beta^{+}} \Gamma(x, y), & (x, y) \in \Omega^{+}. \end{cases}$$
 (5.5)

We test the high coefficient jump cases $(\beta^-, \beta^+) = (1, 1000)$ and $(\beta^-, \beta^+) = (1000, 1)$, and the error tables are reported in Table 3, and Table 4, respectively. The numerical solutions on the 128×128 mesh are plotted in Figure 5. From these data, we can observe again that the error in H^1 - and L^2 -norms converge in first and second order, respectively. And the infinity norm for u_0 and u_b are close to second order and first order.

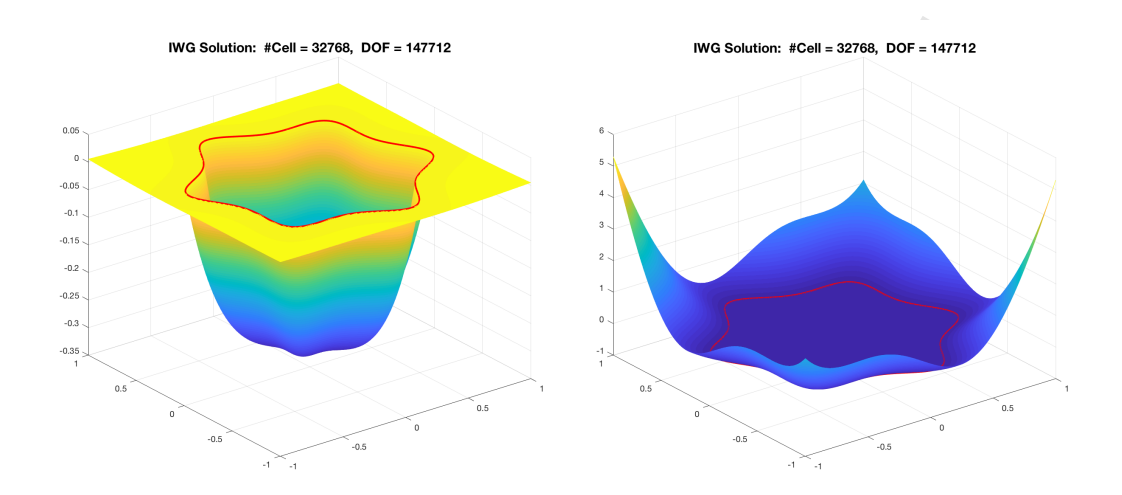


Figure 5: Immersed Weak Galerkin solutions for Example 2 with $(\beta^-, \beta^+) = (1, 1000)$, and $(\beta^-, \beta^+) = (1000, 1)$

N	DOF	$ e_0 _{L^\infty}$	Order	$ e_b _{L^{\infty}}$	Order	$ e_0 _{L^2}$	Order	$ e_0 _{H^1}$	Order
16	2.34E+3	5.00E-2		1.79E-2		8.46E-3		2.89E-1	
32	9.28E+3	1.53E-2	1.71	1.58E-2	0.18	2.30E-3	1.88	1.51E-1	0.94
64	3.70E+4	4.36E-3	1.81	7.68E-3	1.04	5.87E-4	1.97	7.51E-2	1.01
128	1.48E+5	1.38E-3	1.66	4.63E-3	0.73	1.60E-4	1.88	3.68E-2	1.03
256	5.90E+5	4.36E-4	1.66	2.43E-3	0.93	4.07E-5	1.97	1.86E-2	0.99
512	2.26E+6	1.36E-4	1.68	1.18E-3	1.04	1.03E-5	1.99	9.21E-3	1.01
1024	9.44E+6	3.98E-5	1.77	6.00E-4	0.98	2.60E-6	1.98	4.58E-3	1.01

Table 3: Errors of Immersed WG methods Petal Interface for $\beta^- = 1$, $\beta^+ = 1000$

5.3. Example 3

In this example, we consider the case when the interface has a sharp corner. This example has been used in [22]. Let $\Omega = (-1, 1) \times (-1, 1)$, and the interface is defined by the level-set function:

$$\Gamma(x,y) = -y^2 + ((x-1)\tan(\theta))^2 x. \tag{5.6}$$

The subdomains are defined as $\Omega^+ = \{(x, y) : \Gamma(x, y) > 0\}$, and $\Omega^- = \{(x, y) : \Gamma(x, y) < 0\}$. The exact solution is chosen as:

$$u = \begin{cases} \frac{1}{\beta^{-}} \Gamma(x, y), & (x, y) \in \Omega^{-}, \\ \frac{1}{\beta^{+}} \Gamma(x, y), & (x, y) \in \Omega^{+}. \end{cases}$$
 (5.7)

The right hand function f is chosen accordingly to fit the exact solution u in (5.7). We note that on the point (1,0), the interface curve has a sharp corner. We slightly adjust our uniform mesh such that an odd number of partition in each direction. By doing this, the singular point will be located in one of the mesh point. The performance of our proposed numerical scheme is reported in Table 5 and Table 6. Similar conclusions as previous ones can be made for such convergence tests. Furthermore, the numerical solutions are plotted in Figure 6 for varying values in β .

N	DOF	$ e_0 _{L^\infty}$	Order	$ e_b _{L^{\infty}}$	Order	$ e_0 _{L^2}$	Order	$ e_0 _{H^1}$	Order
16	2.34E+3	1.40E-1		3.85E-2		3.01E-2		9.50E-1	
32	9.28E+3	3.81E-2	1.88	1.68E-2	1.20	7.86E-3	1.93	4.84E-1	0.97
64	3.70E+4	9.86E-3	1.95	8.03E-3	1.06	2.02E-3	1.96	2.43E-1	0.99
128	1.48E+5	2.51E-3	1.98	4.64E-3	0.79	5.06E-4	1.99	1.21E-2	1.00
256	5.90E+5	7.41E-4	1.76	2.43E-3	0.93	1.26E-4	2.01	6.07E-2	1.00
512	2.26E+6	1.58E-4	2.23	1.19E-3	1.03	3.15E-5	2.00	3.03E-2	1.00
1024	9.44E+6	3.97E-5	2.00	6.01E-4	0.98	7.87E-6	2.00	1.52E-2	1.00

Table 4: Errors of Immersed WG methods Petal Interface for $\beta^- = 1$, $\beta^+ = 1000$

N	DOF	$ e_0 _{L^\infty}$	Order	$\ e_b\ _{L^\infty}$	Order	$ e_0 _{L^2}$	Order	$ e_0 _{H^1}$	Order
17	2.64E+3	6.55E-2		1.72E-2		1.65E-2		4.88E-1	
33	9.87E+3	1.77E-2	1.89	7.47E-3	1.20	4.41E-3	1.90	2.52E-1	0.95
65	3.82E+4	4.60E-3	1.94	5.15E-3	0.54	1.11E-3	1.98	1.28E-1	0.98
129	1.50E+5	1.17E-3	1.97	2.44E-3	1.08	2.75E-4	2.02	6.45E-2	0.99
257	5.95E+5	2.96E-4	1.99	1.27E-3	0.95	6.88E-5	2.00	3.24E-3	0.99
513	2.37E+6	7.44E-5	1.99	6.96E-4	0.86	1.71E-5	2.00	1.62E-3	1.00
1025	9.46E+6	1.87E-5	2.00	3.56E-4	0.97	4.28E-6	2.00	8.11E-3	1.00

Table 5: Errors of Immersed WG methods Singular Interface for $\beta^- = 1$, $\beta^+ = 1000$

References

- [1] S. Adjerid, N. Chaabane, and T. Lin. An immersed discontinuous finite element method for stokes interface problems. *Comput. Methods Appl. Mech. Engrg.*, 293:170–190, 2015.
- [2] S. Adjerid, R. Guo, and T. Lin. High degree immersed finite element spaces by a least squares method. *Int. J. Numer. Anal. Model.*, 14(4-5):604–626, 2017.
- [3] D. N. Arnold, F. Brezzi, B. Cockburn, and L. D. Marini. Unified analysis of discontinuous Galerkin methods for elliptic problems. SIAM J. Numer. Anal., 39(5):1749–1779, 2002.
- [4] L. Beirão da Veiga, F. Brezzi, A. Cangiani, G. Manzini, L. D. Marini, and A. Russo. Basic principles of virtual element methods. *Math. Models Methods Appl. Sci.*, 23(1):199–214, 2013.
- [5] L. Beirão da Veiga, F. Brezzi, L. D. Marini, and A. Russo. Virtual element method for general second-order elliptic problems on polygonal meshes. *Math. Models Methods Appl. Sci.*, 26(4):729–750, 2016.
- [6] J. H. Bramble and J. T. King. A finite element method for interface problems in domains with smooth boundaries and interfaces. Adv. Comput. Math., 6(2):109–138, 1996.
- [7] E. Burman, S. Claus, P. Hansbo, M. G. Larson, and A. Massing. CutFEM: discretizing geometry and partial differential equations. *Internat. J. Numer. Methods Engrg.*, 104(7):472–501, 2015.
- [8] W. Cao, X. Zhang, and Z. Zhang. Superconvergence of immersed finite element methods for interface problems. Adv. Comput. Math., 43(4):795–821, 2017.
- [9] W. Cao, X. Zhang, Z. Zhang, and Q. Zou. Superconvergence of immersed fnite volume methods for one-dimensional interface problems. *J. Sci. Comput.*, 73(2-3):543–565, 2017.

N	DOF	$ e_0 _{L^\infty}$	Order	$ e_b _{L^{\infty}}$	Order	$ e_0 _{L^2}$	Order	$ e_0 _{H^1}$	Order
17	2.64E+3	1.48E-2		1.49E-2		2.41E-3		8.58E-2	
33	9.87E+3	5.79E-3	1.36	8.62E-3	0.79	6.73E-4	1.84	4.42E-2	0.96
65	3.82E+4	2.17E-3	1.42	5.30E-3	0.70	1.69E-4	2.00	2.28E-2	0.95
129	1.50E+5	5.20E-4	2.06	2.46E-3	1.11	3.80E-5	2.15	1.09E-2	1.06
257	5.95E+5	1.21E-4	2.10	1.27E-3	0.95	9.25E-6	2.04	5.48E-3	1.00
513	2.37E+6	3.14E-5	1.95	6.95E-4	0.87	2.25E-6	2.04	2.71E-3	1.01
1025	9.46E+6	8.06E-6	1.96	3.56E-4	0.97	5.58E-7	2.01	1.36E-3	1.00

Table 6: Errors of Immersed WG methods Singular Interface for $\beta^-=1000, \beta^+=1$

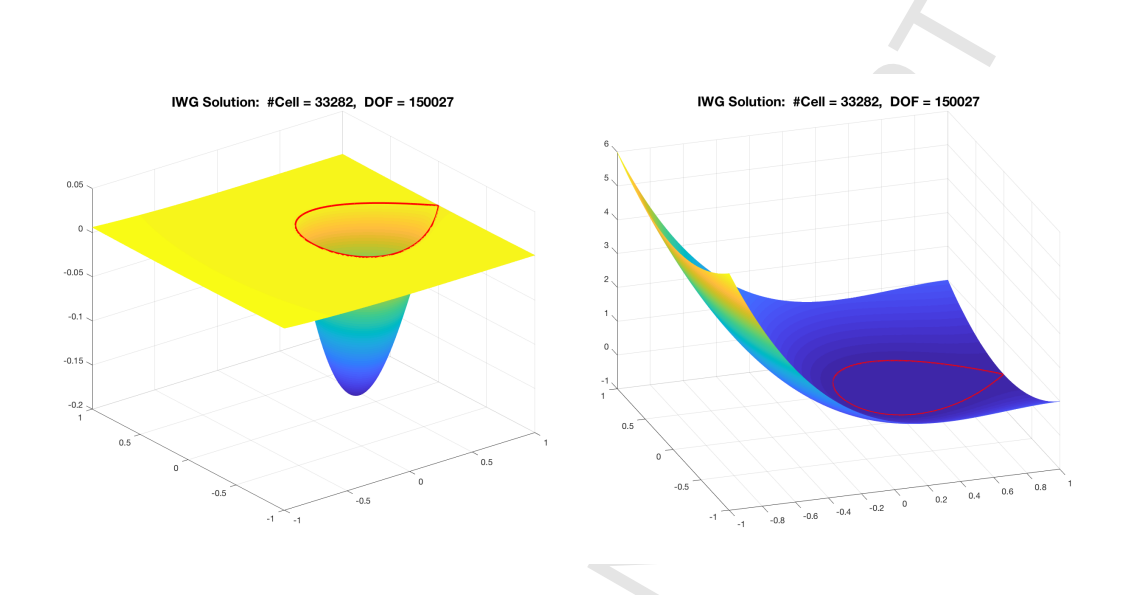


Figure 6: Immersed Weak Galerkin solutions for Example 3 with $(\beta^-, \beta^+) = (1, 1000)$, and $(\beta^-, \beta^+) = (1000, 1)$

- [10] Z. Chen and J. Zou. Finite element methods and their convergence for elliptic and parabolic interface problems. Numer. Math., 79(2):175–202, 1998.
- [11] C.-C. Chu, I. G. Graham, and T.-Y. Hou. A new multiscale finite element method for high-contrast elliptic interface problems. *Math. Comp.*, 79(272):1915–1955, 2010.
- [12] J. Dolbow, N. Moës, and T. Belytschko. An extended finite element method for modeling crack growth with frictional contact. Comput. Methods Appl. Mech. Engrg., 190(51-52):6825-6846, 2001.
- [13] R. E. Ewing, Z. Li, T. Lin, and Y. Lin. The immersed finite volume element methods for the elliptic interface problems. *Math. Comput. Simulation*, 50(1-4):63–76, 1999. Modelling '98 (Prague).
- [14] R. Guo, T. Lin, and X. Zhang. Nonconforming immersed finite element spaces for elliptic interface problems. Comput. Math. Appl., 75(6):2002–2016, 2018.
- [15] A. Hansbo and P. Hansbo. An unfitted finite element method, based on Nitsche's method, for elliptic interface problems. Comput. Methods Appl. Mech. Engrg., 191(47-48):5537–5552, 2002.
- [16] X. He, T. Lin, and Y. Lin. A bilinear immersed finite volume element method for the diffusion equation with discontinuous coefficient. Commun. Comput. Phys., 6(1):185–202, 2009.
- [17] X. He, T. Lin, and Y. Lin. A selective immersed discontinuous Galerkin method for elliptic interface problems. Math. Methods Appl. Sci., 37(7):983–1002, 2014.
- [18] X. He, T. Lin, Y. Lin, and X. Zhang. Immersed finite element methods for parabolic equations with moving interface. Numer. Methods Partial Differential Equations, 29(2):619–646, 2013.
- [19] S. Hou and X.-D. Liu. A numerical method for solving variable coefficient elliptic equation with interfaces. J. Comput. Phys., 202(2):411–445, 2005.
- [20] S. Hou, W. Wang, and L. Wang. Numerical method for solving matrix coefficient elliptic equation with sharp-edged interfaces. J. Comput. Phys., 229(19):7162–7179, 2010.
- [21] T. Y. Hou, X.-H. Wu, and Z. Cai. Convergence of a multiscale finite element method for elliptic problems with rapidly oscillating coefficients. *Math. Comp.*, 68(227):913–943, 1999.
- [22] D. Y. Kwak, K. T. Wee, and K. S. Chang. An analysis of a broken P₁-nonconforming finite element method for interface problems. SIAM J. Numer. Anal., 48(6):2117–2134, 2010.
- [23] R. J. LeVeque and Z. L. Li. The immersed interface method for elliptic equations with discontinuous coefficients and singular sources. SIAM J. Numer. Anal., 31(4):1019–1044, 1994.
- [24] Z. Li. The immersed interface method using a finite element formulation. Appl. Numer. Math., 27(3):253-267, 1998.
- [25] Z. Li and K. Ito. The immersed interface method, volume 33 of Frontiers in Applied Mathematics. Society for Industrial and Applied Mathematics (SIAM), Philadelphia, PA, 2006. Numerical solutions of PDEs involving interfaces and irregular domains.

- [26] Z. Li, T. Lin, Y. Lin, and R. C. Rogers. An immersed finite element space and its approximation capability. Numer. Methods Partial Differential Equations, 20(3):338–367, 2004.
- [27] Z. Li, T. Lin, and X. Wu. New Cartesian grid methods for interface problems using the finite element formulation. *Numer. Math.*, 96(1):61–98, 2003.
- [28] T. Lin, Y. Lin, R. Rogers, and M. L. Ryan. A rectangular immersed finite element space for interface problems. In Scientific computing and applications (Kananaskis, AB, 2000), volume 7 of Adv. Comput. Theory Pract., pages 107–114. Nova Sci. Publ., Huntington, NY, 2001.
- [29] T. Lin, Y. Lin, and X. Zhang. A method of lines based on immersed finite elements for parabolic moving interface problems. Adv. Appl. Math. Mech., 5(4):548–568, 2013.
- [30] T. Lin, Y. Lin, and X. Zhang. Partially penalized immersed finite element methods for elliptic interface problems. SIAM J. Numer. Anal., 53(2):1121–1144, 2015.
- [31] T. Lin, D. Sheen, and X. Zhang. A locking-free immersed finite element method for planar elasticity interface problems. J. Comput. Phys., 247:228–247, 2013.
- [32] T. Lin, D. Sheen, and X. Zhang. Nonconforming immersed finite element methods for elliptic interface problems. (arXiv:1510.00052).
- [33] T. Lin, Q. Yang, and X. Zhang. A Priori error estimates for some discontinuous Galerkin immersed finite element methods. J. Sci. Comput., 65(3):875–894, 2015.
- [34] T. Lin and X. Zhang. Linear and bilinear immersed finite elements for planar elasticity interface problems. *J. Comput. Appl. Math.*, 236(18):4681–4699, 2012.
- [35] J. Liu, S. Tavener, Z. Wang. The Lowest-order Weak Galerkin Finite Element Method for the Darcy Equation on Quadrilateral and Hybrid Meshes. *Journal of Computational Physics*, 2018.
- [36] N. Moës, J. Dolbow, and T. Belytschko. A finite element method for crack growth without remeshing. *Internat. J. Numer. Methods Engrg.*, 46(1):131–150, 1999.
- [37] L. Mu, J. Wang, Y. Wang, and X. Ye. A computational study of the weak Galerkin method for second-order elliptic equations. *Numer. Algorithms*, 63(4):753–777, 2013.
- [38] L. Mu, J. Wang, G. Wei, X. Ye, and S. Zhao. Weak Galerkin methods for second order elliptic interface problems. *J. Comput. Phys.*, 250:106–125, 2013.
- [39] L. Mu, J. Wang, and X. Ye. Weak Galerkin finite element methods on polytopal meshes. International Journal of Numerical Analysis & Modeling, 12:31-53, 2015.
- [40] L. Mu, J. Wang, X. Ye, and S. Zhao. A new weak galerkin finite element method for elliptic interface problems. *Journal of Computational Physics*, 325:157–173, 2016.
- [41] B. Rivière, M. F. Wheeler, and V. Girault. Improved energy estimates for interior penalty, constrained and discontinuous Galerkin methods for elliptic problems. I. *Comput. Geosci.*, 3(3-4):337–360 (2000), 1999.
- [42] J. Wang and X. Ye. A weak Galerkin finite element method for second-order elliptic problems. J. Comput. Appl. Math., 241:103-115, 2013.
- [43] L. Zhu, Z. Zhang, and Z. Li. The immersed finite volume element method for some interface problems with nonhomogeneous jump conditions. Int. J. Numer. Anal. Model., 13(3):368–382, 2016.